Collision dynamics of binary liquid metal droplets under horizontal magnetic field

Xiao Jia,[1,3,*] Juan-Cheng Yang ⬤,[2,*] Jie Zhang,[2] Long Chen,[1] and Ming-Jiu Ni ⬤[1,2,†]

[1]*School of Engineering Science, University of Chinese Academy of Sciences, Beijing 101408, China*
[2]*State Key Laboratory for Strength and Vibration of Mechanical Structures, School of Aerospace, Xi'an Jiaotong University, Xi'an 710049, China*
[3]*Institute of Engineering Thermophysics, Chinese Academy of Sciences, Beijing 100190, China*

The present paper aims to investigate the magnetohydrodynamic effects on binary liquid metal droplet collision in the presence of horizontal magnetic field ($0 < B < 1.5$ T) normal to collision velocity. Here we observe that for small magnetic interaction parameter N (<0.4), one type of collision regimes, reflexive separation, could be obviously facilitated by magnetic field in comparison with no magnetic cases. For collision regimes except reflexive separation, we present a correlation of $N = f(B/B_0, \mathrm{We}/48)$ as well as a N-We/48 map that could help to interpret why little influence of magnetic field on them and predict possible remarkable influences when B is larger than a critical value of 4 T. Furthermore, we draw the possible geometrical morphology of droplets after collision based on our understanding of the physical process of liquid metal droplets collision under the horizontal magnetic field.

I. INTRODUCTION

Providing efficacious first wall materials between the extreme plasma heat exhaust and the solid structural frameworks of nuclear fusion devices is a major challenge on the road to electricity production by fusion power plants [1,2]. One promising solution is to maintain a constantly recycled thin film of liquid metal (typically lithium) to cover and protect the solid substrate [3]. Nowadays, liquid metal has been proposed as one of the most promising first wall materials for divertor, limiter, and plasma-facing components (PFCs) in fusion reactors, due to its overwhelming advantages over solid materials, such as self-regenerating and continuously flowing, high-power conversion efficiency, large bombardment capability, wide temperature range, and possible stabilization of magnetohydrodynamic (MHD) modes, etc. [4–8]. However, an outstanding concern over adoption of liquid metal is the potential of droplets ejecting or splashing from the liquid surface into the plasma core area [9,10]. Under the presence of high-speed plasma bombardment and ultrastrong heat load, the flowing liquid metal is apt to eject, which might be caused by boiling and explosion of gas bubbles, absorption of plasma momentum, current-induced Lorentz forces, and Rayleigh-Taylor or Kelvin-Helmholtz instabilities, etc. [11–13]. In the presence of high magnetic field, the situation would be more serious, and such possibilities are exemplified in the following works: Hassanein [14] theoretically predicted that splashing of macroscopic metal droplets from liquid surface results in the ablation of PFC materials. Whyte *et al.* [15] observed in experiments of DIII-D tokamak divertors that vertical injection of lithium droplets into a reactor core is caused by radial electric current

---

*These authors contributed equally to this work.
†Corresponding author: mjni@ucas.ac.cn

TABLE I. Properties of several types of metal.

Liquid	ρ (kg/m^3)	μ (mPa×s)	σ (mN/m)	σ_e (S/m)	Melting point (°C)	Speciality
Mercury	13610	1.53	460	1.0×10^6	−39	Toxic
Alumina	2686	14.8	615	−	2054	Solid
Lithium	515	0.57	390	3.626×10^6	180	Explosive
GaInSn	6360	1.9	533	3.27×10^6	−19	Nontoxic

and toroidal magnetic field. Rudolph and Miloshevsky [16] discovered the growth of small liquid lithium ripples and their disintegration into droplets occurred at very high speed of plasma by using both analytical method and computational modeling. For all of them, the ejected droplets would cause immediate exposure of underlying structural materials and result in direct radiation damage from high-powered plasma discharges, which would severely limit a divertor system's lifetime and significantly contaminate plasma in a reactor core [17,18]. In addition, random collisions between the ejected liquid metal droplets massively appear, causing a major hazard on the plasma reaction environment in the core and threatening the sustainability of whole system, but it is still unclear what would happen when two liquid metal droplets collide under the influence of magnetic field. Therefore, it is quite necessary to carry out the experiment of liquid metal droplet collision under the influence of magnetic field for its critical importance in achieving a controllable and safe fusion reactor system.

For liquid metal droplet collision without magnetic field, Menchaca-Rocha *et al.* [19] have experimentally studied the collision of two mercury droplets falling from two 30° ramps to a specially treated horizontal glass surface. They presented a surface-dynamic nuclear fragmentation model for macroscopic droplet collision (*D* up to 5 mm). However, the nonspherical shape before collision brought confusion on whether the deformation of collision results from initial shape or collision itself. Besides, Xia *et al.* [20,21] have numerically investigated head-on and off-center collisions of alumina droplets at 3387 K, while the experiment couldn't be carried out due to ultrahigh temperature. For nuclear reactors, lithium has been identified as the potential solution for PFC materials, however, for experiments in a laboratory, room-temperature liquid metal GaInSn is more preferred, owing to its stable and nontoxic characteristics compared with the above-mentioned several types of liquid metal. All their properties are presented in Table I.

In our previous study, without applying magnetic field [22], we have conducted detailed experiments on the dynamics of GaInSn droplet collisions in a wide range covering Weber numbers (We) from 5 to 400 and impact parameters (*X*) from 0 to 1. Six different collision types are identified: coalescence, stretching separation, coalescence after finger, separation of finger, breakup after finger, and stretching separation with finger pinching. We found that both collision regimes in low We range (without finger generation) and in high We range (with finger generation) could be observed in a relatively small range (We < 400) compared with other ordinary liquids. Under the influence of magnetic field, droplet collisions may also be greatly different from ordinary liquids due to liquid metal's large surface tension coefficient and induced Lorentz force inside. Herein, the schematic view for this problem is illustrated in Fig. 1. Generally, the phenomenon of binary droplet collision could be described by two parameters: the Weber number We, being the ratio of inertia and surface tension, and the impact parameter *X*, indicating the degree to which the collision is off center. For collisions of different liquid droplets with various viscosities to be compared, Ohnesorge number Oh is needed, which demonstrates the ratio of viscous force and the combined effect of inertia and surface tension. In addition, when an external magnetic field is imposed, another dimensionless parameter, magnetic interaction parameter *N*, defining the ratio between electromagnetic force and inertial force, needs to be considered. They are defined as follows:

$$\text{We} = \frac{\rho D U^2}{\sigma}; \quad X = \frac{x}{D}; \quad \text{Oh} = \frac{\mu}{\sqrt{\rho \sigma D}}; \quad N = \frac{\sigma_e D B^2}{\rho U}, \tag{1}$$
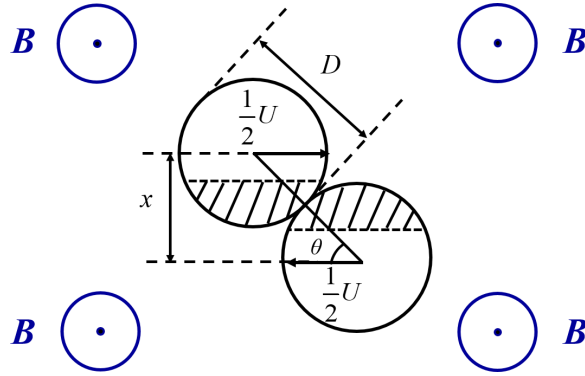
FIG. 1. Schematic view of the collision between two droplets under horizontal magnetic field.

where ρ is the density of liquid, σ is surface tension coefficient, μ is dynamic viscosity, D is droplet diameter, U is the relative velocity of two droplets, x is the distance between two droplet centers in the line perpendicular to relative velocity before the moment of colliding, σ_e is electrical conductivity, and B is magnetic field intensity, whose direction is perpendicular to the initial relative velocity of binary droplets in this paper.

The major objectives of this paper are to answer the following questions: (1) How does the magnetic field influence collision outcomes of liquid metal droplets? (2) What parameters, and their values, define the influencing extent of magnetic field on collision regimes? To answer these questions, this paper is organized as follows: Experimental apparatus and methods are presented in Sec. II, then a general simple analysis of collision outcomes under magnetic field is presented in Sec. III A, results including successive snapshots and classifications of various collision outcomes in Sec. III B, influence of magnetic field on reflexive separation in Sec. III C, and reasons why little influence on other collision regimes and possible collision processes when the intensity of magnetic field larger than 4 T in Sec. III D. Finally, this paper ends with conclusion.

II. EXPERIMENTAL SYSTEM AND METHODS

The 3D model of experimental system and detailed arrangement of mirrors, light source, and camera are shown in Fig. 2. Here two droplet generators are used to produce two streams of the same-sized droplets in free flight to collide. They are mounted with two electromechanical arms onto an optical platform, which could be moved in x, y, z directions and rotated in $x - o - y$ plane precisely. The apparatus is sealed in a specially made plexiglass chamber with Ar gas being inlet before experiment to prevent oxidation of GaInSn droplets. Two droplet streams collide on a vertical plane and their collision processes are recorded by a high-speed camera horizontally. However, it should be noted that the external dimension of a single droplet generator is 48 mm but the width of magnetic field gap is 80 mm. It's unable to put two droplet generators in the width direction parallel with magnetic field, but only be put along the direction perpendicular to magnetic field. Therefore, two reflective mirrors fixed parallelly in 45° position above the liquid reservoir are needed to record image, as is shown in Figs. 2(b) and 2(c), allowing the visualization of the collision phenomenon from a perpendicular direction.

During experiments, one stream of equal-sized droplets is first manipulated to the focal plane of high-speed camera, where the droplet contours are clearest, and the other stream is manipulated to a close parallel plane. The parallelism of two streams could be verified through their falling traces. By adjusting the position of second stream to go across camera's focal plane (from one side to the other), streams of droplets collide and numerous images could be collected. After experiments, qualified collisions with clearest contour and perfect shape are picked out from raw data. For a
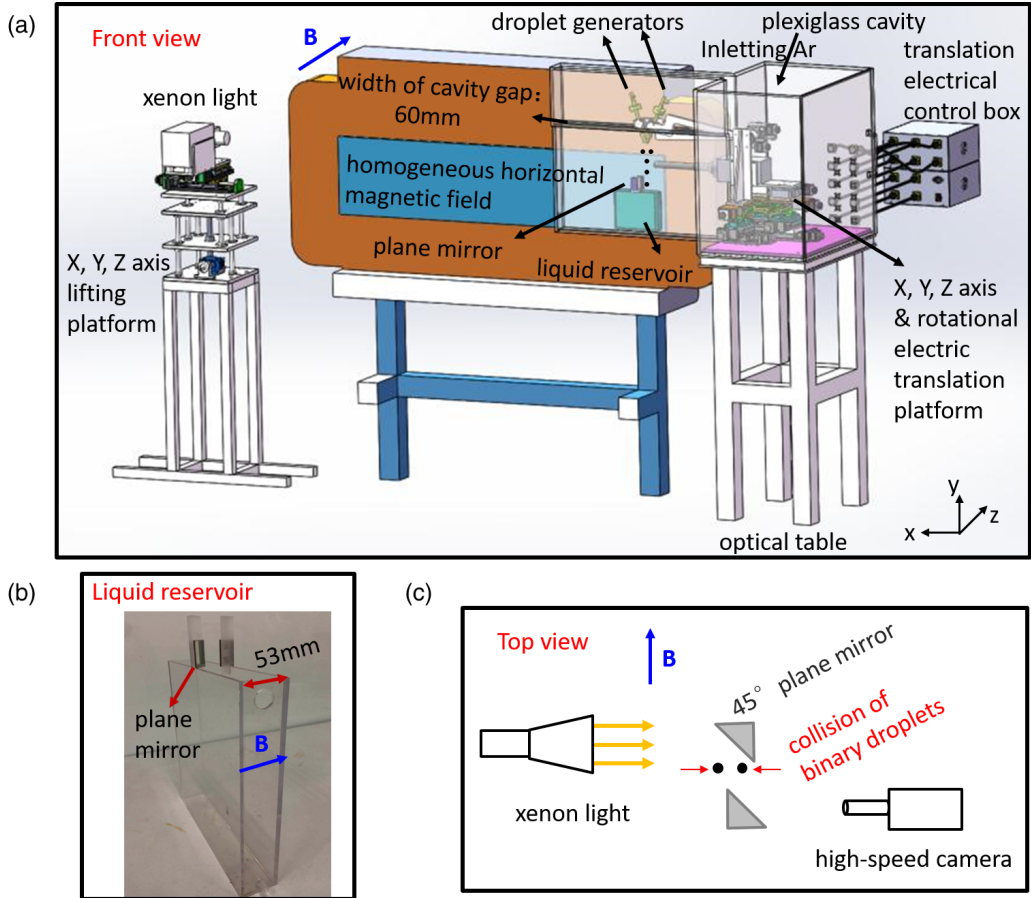
FIG. 2. (a) Sketch of the experimental setup. (b) Photo of liquid reservoir. (c) Top view of image-forming principle by $45°$ plane mirror.

specific pair, droplet diameter and relative velocity could be acquired from the last two shots before colliding, and then we can get We and X. More detailed experimental and postprocessing procedures can be found in our previous paper [22].

III. PREDICTION, RESULTS AND DISCUSSION

A. Qualitative prediction on binary collision with magnetic field

Even though droplet collision under imposed magnetic field has never been carried out before, a few experiments of droplet impacting onto a solid plate under magnetic field could provide some qualitative and quantitative results. For example, Zhang *et al.* [23] developed a theoretical model by numerical simulation to predict the maximum spreading diameter of an impacting droplet under vertical magnetic field. The induced Lorentz force, which acts as a resistance to spreading, will diminish the maximum spreading radius. Yang *et al.* [24] observed in experiments that a liquid metal droplet shows anisotropic spread characteristics onto a glass surface under horizontal magnetic field. Magnetic field promotes spreading in its perpendicular direction while it reduces spreading along it, resulting in elliptical spreading.

All these results show the magnetic field has an effect on the deformation and motion of liquid metal droplets when it interacts with other mediums and, particularly, the direction of magnetic field
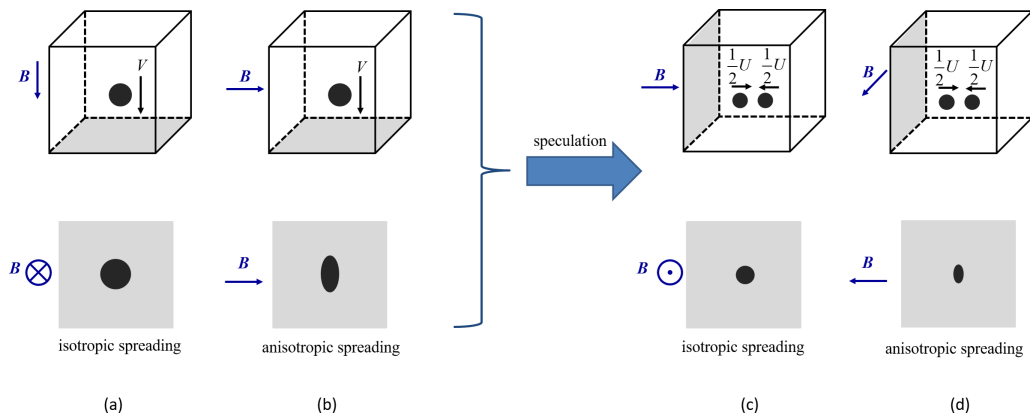
FIG. 3. Schematic of the speculation of effects of magnetic field on binary collision from droplet impacting onto solid plate: (a) a single droplet impact onto a plate under vertical magnetic field; (b) a single droplet impact onto a plate under horizontal magnetic field; (c), (d) binary droplet collision under horizontal magnetic field: (c) the direction of magnetic field is parallel with relative velocity of two droplets, (d) the direction of magnetic field is perpendicular to relative velocity of two droplets.

is a key factor in determining the spreading process and final state of the droplet, see Fig. 3. For the vertical magnetic field in Fig. 3(a), the spreading diameter is reduced uniformly and isotropically. For the horizontal magnetic field in Fig. 3(b), the droplet spreads in an elliptical pattern. Under horizontal magnetic field, the nonuniform distribution of the Lorentz force in the radial direction is the main reason to cause elliptical spreading phenomenon. This paper mainly focuses on the effects of the horizontal magnetic field on the collision of binary liquid metal droplets. It could be inferred that the spreading of two colliding droplets might be uniformly inhibited if the initial relative velocity is parallel with magnetic field but anisotropically distributed in the perpendicular case. Due to limited space, Fig. 3(c) couldn't be obtained in our experiments, while Fig. 3(d), where the direction of horizontal magnetic field is perpendicular to the relative velocity, could be achieved.

To quantitatively figure out the influence of magnetic field, it's useful to compare the parameters in different works. Table II shows the parameters of this experiment in comparison with simulations and experiments done by Zhang *et al.* [23] and Yang *et al.* [24], which demonstrates the magnitude of magnetic interaction parameter N in their works is 1 to 2 times larger than ours. Therefore, we infer that small N in our experiments might not induce large electromagnetic influences, while it may exert some effects on collision regimes when deformation of droplets is significant in the plane perpendicular to magnetic field. In the following, the experimental results are generally consistent with our prediction.

B. Collisional regimes

Six representative collisions of GaInSn droplets when intensity of magnetic field is 1.5 T are shown in Fig. 4, namely, (a) coalescence, (b) reflexive separation, (c) coalescence after finger,

TABLE II. Parameters of simulation and experiment for comparison.

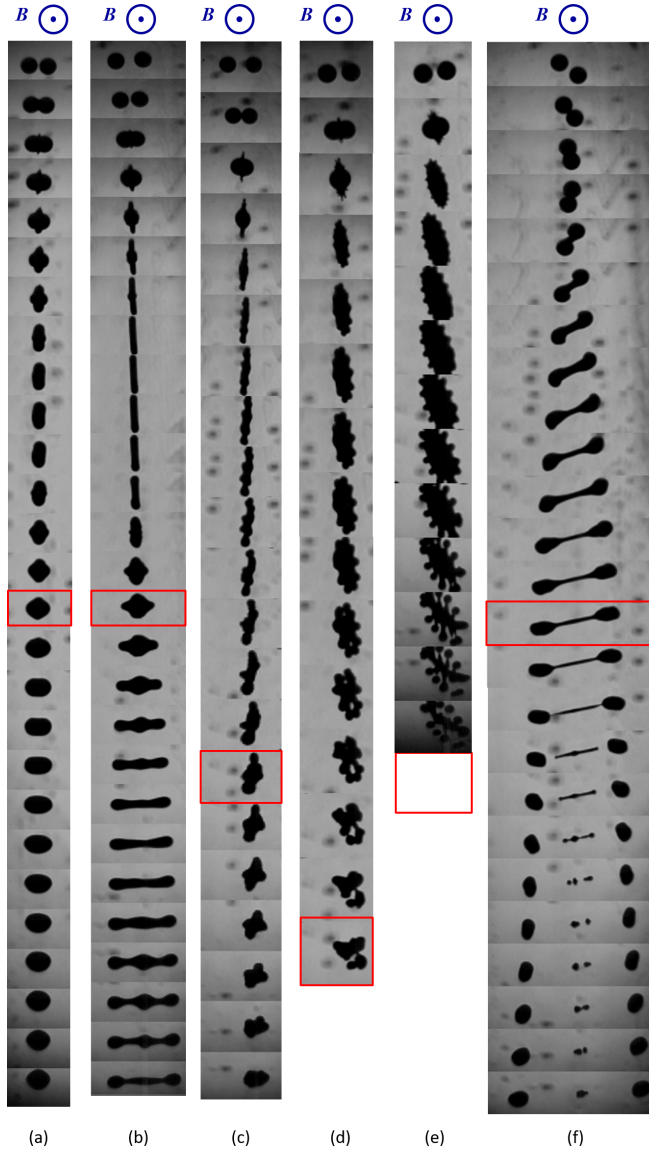| Reference	Method	D (μm)	V or U (m/s)	B (T)	We	N
Zhang *et al.* [23]	Simulation	2000	0.6−6	0−6	20−100	0 − 16
Yang *et al.* [24]	Experiment	2300	0.1−1.2	0−2	0.2−46	0−3.73
This paper	Experiment	336−418	1−7	0−1.5	0−200	0−0.4

FIG. 4. The snapshots of different colliding processes for $B = 1.5$ T. Every sequence is a specific pair of droplets cut out from continuous shots. (a) Coalescence, We = 12.84, $X = 0.1787$, $D = 424$ μm, $U = 1.593$ m/s; (b) reflexive separation, We = 50.13, $X = 0.0088$, $D = 428$ μm, $U = 3.132$ m/s; (c) coalescence after finger, We = 110.90, $X = 0.0996$, $D = 436$ μm, $U = 4.615$ m/s; (d) separation of finger, We = 121.73, $X = 0.0579$, $D = 446$ μm, $U = 4.785$ m/s; (e) break-up after finger, We = 187.08, $X = 0.0431$, $D = 425$ μm, $U = 6.0724$ m/s; and (f) stretching separation, We = 55.69, $X = 0.8565$, $D = 403$ μm, $U = 4.8951$ m/s. The interval between two snapshots is $1/18\,000$ s. The red rectangular represents the 0.8 ms moment after impact, which is the characteristic time of obvious difference for reflexive separation with magnetic field. The detailed information on the characteristic time of 0.8 ms is discussed in Sec. III D.

(d) separation of finger, (e) breakup after finger and (f) stretching separation. Figure 5 shows the regions of different types of collision regimes with and without magnetic field for the range of $0 < X < 1$ and $5 <$ We < 200, where the above-mentioned six regimes appear in five distinct regions
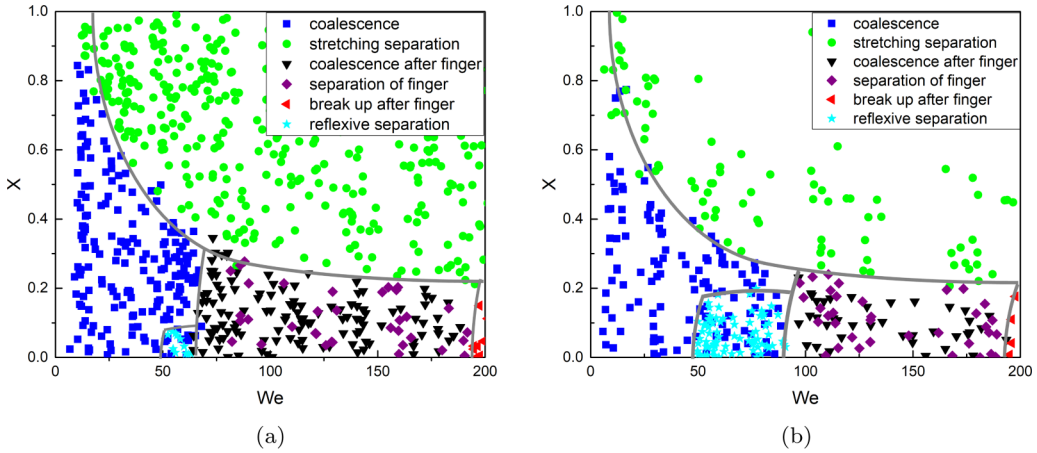
FIG. 5. Maps of regimes for binary collision of same-sized GaInSn droplets with and without magnetic field. The droplet diameter ranges from 336 to 418 μm. The relative velocity is varied from 1 to 7 m/s. (a) B = 0 T and (b) B = 1.5 T.

and their boundaries are empirically drawn with gray lines. The former five types [Figs. 4(a)–4(e)] are generally observed in the low X range while the latter one Fig. 4(f) is more likely to appear in relatively high X range.

Coalescence occurs in the region with blue squares in the low We range of Fig. 5: after two droplets contact, the merged droplet deforms slightly and generates a thick claylike structure, as shown in Fig. 4(a), which would finally oscillate from an ellipsoidal shape to spherical shape. As We increases, the collision complex has undergone small deformation to large deformation of generating a circular sheet, as shown in Fig. 4(b). If there is still enough kinetic energy left after compression, reflexive separation might occur; if not, coalescence would occur. If We number further increases, coalescence after finger occurs with fingers generating around, see Fig. 4(c) and the region with black down-triangles nearly between 90 to 195 in Fig. 5. However, formation of fingers reduces the possibility of separating since insufficient kinetic energy is left, which results in the contraction of collision complex into a merged body. In the same region, separation of finger, similar to the collision process of coalescence after finger, occurs randomly, which is plotted by purple diamonds in Fig. 5, but the difference comes from the contraction phase: When the inner sheet of disk retreats, one or two fingers at the rim separate from the main body and break into satellite droplets, as shown in Fig. 4(d). Since the We number has been in a relatively high range now, the leftover kinetic energy after compression couldn't all be contained in a closed surface. To balance the additional energy, individual fingers (not all) disintegrate into satellite droplets while the main sheet structure still contracts into a whole body. As the We number increases further, all the fingers around the rim would separate into satellite droplets, called breakup after finger, as shown in Fig. 4(e). The corresponding results are plotted in Fig. 5 by red left triangles. All the above-mentioned five regimes generally occur in the low X range, while the sixth collision regime, stretching separation, occurs in the relatively high X range, see the green circles in Fig. 5. When two droplets collide at high X, only a portion of them contact directly while the remaining portions tend to move along the direction of their initial trajectory, stretching the whole collision complex. During stretching process, the inner filament separates from bulbous ends and contracts into several satellite droplets in the middle, as shown in Fig. 4(f). For the same We number, if the impact parameter X increases, separation is more likely to occur since the stretching portion over the interaction portion increases.

We can observe that the collision regime distribution with and without magnetic field doesn't show large differences for most of the regions except one, reflexive separation. Obvious reflexive separation has been observed when We is around 48 under the magnetic field. Therefore, we further
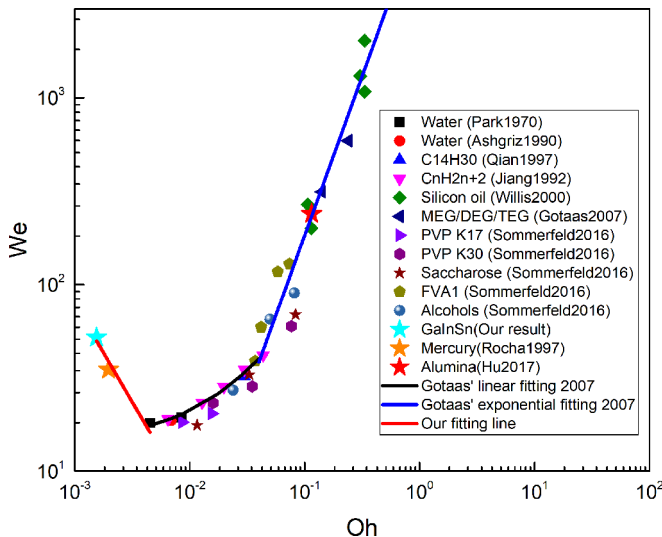
FIG. 6. Onset: We numbers of reflexive separation for different fluids (by adding liquid metal GaInSn, mercury, and alumina droplets) in variance with Oh numbers.

conduct the contrast experiment without magnetic field in detail in this range. A little different from our former work is that we could occasionally observe reflexive separation when We $\approx 52 - 62$, see lake blue stars in Fig. 5(a), however in most cases, coalescence instead of reflexive separation would occur at nearly the same We number, see blue squares in Fig. 5(a). Gotaas *et al.* [25] has empirically concluded a two-segmented fitting line for the onset We number of reflexive separation: linear curve for Oh < 0.04 and exponential curve for Oh > 0.04, but the region for $Oh_{(water)} < 0.00451$, which stands for liquids with large surface tension coefficient and low viscosity (such as liquid metal), has not been considered before. Therefore the onset correlation should be amended by taking liquid metal collision results into account. By adding the Rocha's results of mercury [19] and our results of GaInSn, we modify the onset We number of reflexive separation for smaller Oh numbers, as is shown in Fig. 6 and Eq. (2):

$$
We = \begin{cases} 0.05423Oh^{-1.0545}, & 0.00155 \leqslant Oh < 0.00451 \\ 643.1Oh + 14.8, & 0.00451 \leqslant Oh < 0.04 \\ 9309Oh^{1.7056}, & Oh > 0.04. \end{cases} \tag{2}
$$

In addition, the onset We number for alumina droplets from Xia and Hu's works [20,21] fits well with the exponential line for Oh > 0.04. It demonstrates that the onset We number of reflexive separation for different liquids could totally be divided into three segments: with Oh number increasing, the onset line first decreases and then rises from slow to fast. But when magnetic field is imposed, the reflexive separation occurs more commonly in a wider range around We $\approx 48 - 90$, see Fig. 5(b). More detailed information of reflexive separation and the influence of different magnetic intensities on it is discussed in Sec. III C.

C. Reflexive separation

Reflexive separation is obviously observed under the influence of magnetic field from We ≈ 48 on, where the initial kinetic energy of two same-sized droplets is nearly the same with their surface tension energy (since We/48 $= \frac{\frac{1}{24}\rho\pi D^3 U^2}{2\pi\sigma D^2} = \frac{E_{k0}}{E_{s0}}$). When two equal-sized droplets collide head-on, they form a disklike complex; the disk will therefore contract radially inward and then generate
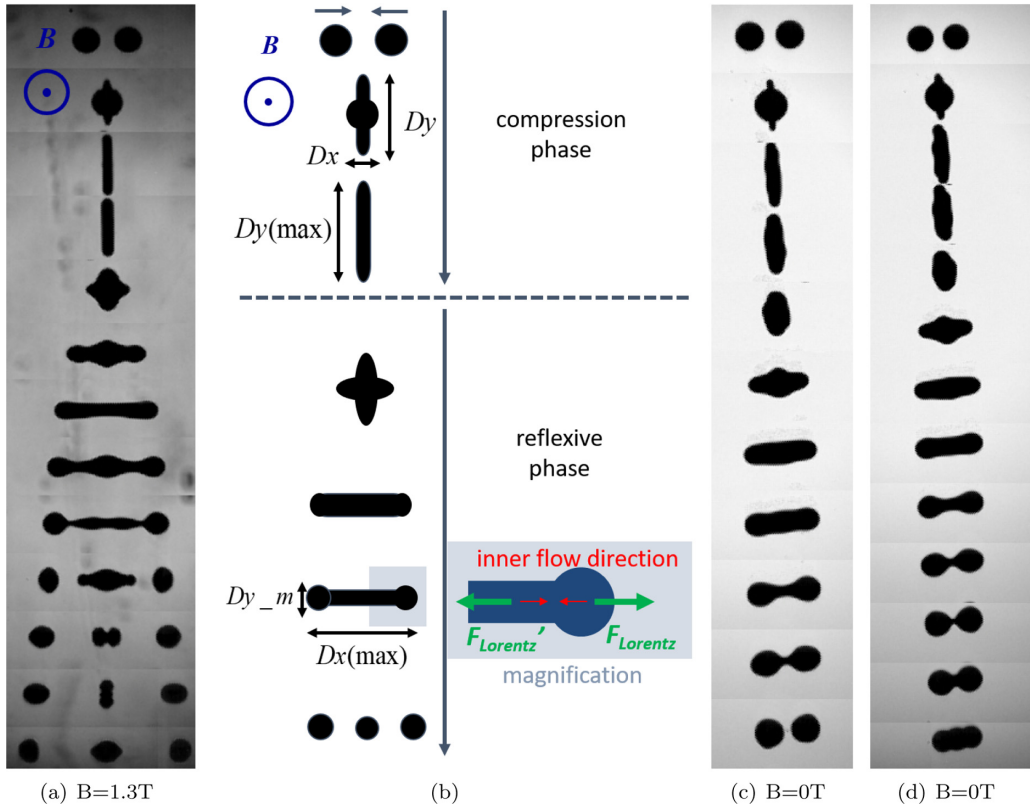
FIG. 7. (a) Collision outcome of reflexive separation for same-sized GaInSn droplets under imposed magnetic field of 1.3 T. We = 60.25, $X = 0.0186$, $D = 414$ μm, $U = 3.494$ m/s. (b) Schematic of reflexive separation changes over time. (c) Collision outcome of reflexive separation for same-sized GaInSn droplets without magnetic field. We = 61.77, $X = 0.0094$, $D = 427$ μm, $U = 3.481$ m/s. (d) Collision outcome of coalescence for same-sized GaInSn droplets without magnetic field. We = 63.41, $X = 0.0790$, $D = 415$ μm, $U = 3.579$ m/s. For (a), (c), and (d), the interval between two snapshots is $3 \times 1/18000$ s.

a long cylinder with rounded ends. After two rounded ends separate, one satellite formed in the middle would go through large oscillations until it becomes spherical, see Fig. 7(a). As done by Jiang *et al.* [26] and Planchette *et al.* [27], we also subdivide reflexive separation into two phases: a compression phase and reflexive phase. The schematic of evolutionary process is presented in Fig. 7(b) in contrast to snapshots in Fig. 7(a). The first phase extends from the instant of impact to the state of maximum extension, during which the combination of two droplets includes radical flow in the spreading lamella and axial flows in almost spherical rear parts of the colliding droplets. The second phase corresponds to the relaxation of deformed entity into a transversely elongated, nearly cylindrical shape. Finally, fragmentation occurs if the cylinder formed during relaxation phase stretches to a critical extent. The contrast experiment without magnetic field shows reflexive separation could occasionally be observed: the collision complex doesn't obviously generate a long ligament structure but only a short joint, see Fig. 7(c), while in most cases coalescence instead of reflexive separation would occur due to insufficient kinetic energy, see Fig. 7(d). When magnetic field is imposed, reflexive separation occurs more easily, where the portion of ligament stretches longer compared to cases without magnetic field, see Fig. 7(a).

Based on Rayleigh's linear theory [28], if the length-to-diameter ratio ζ of a liquid column is equal to π, the column becomes unstable and fragmentation might occur. The Rayleigh criterion,
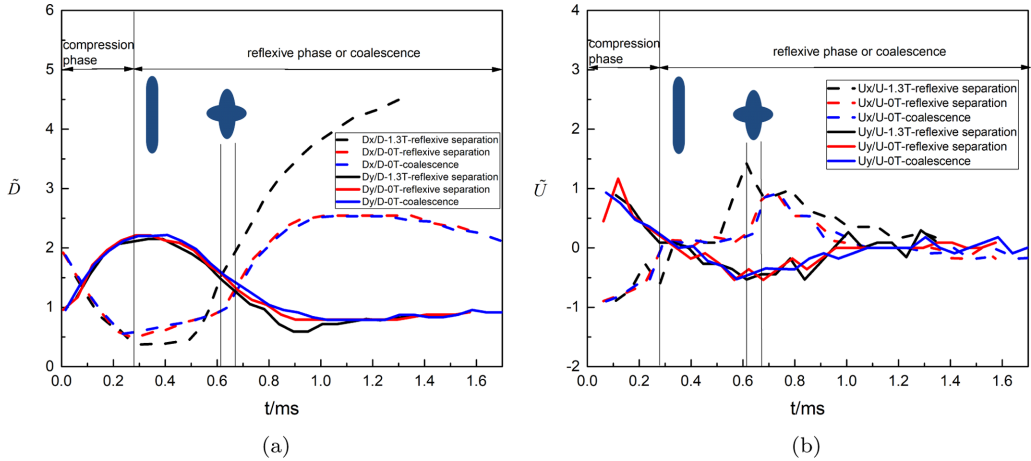
FIG. 8. The spreading diameters D_y and lateral length D_x normalized by droplet diameter D, and U_x, U_y normalized by relative velocity U vary with time t.

normally applied to a static infinite liquid cylinder, was proposed by Ashgriz and Poo [29] for binary collisions of water drops and also used by Planchette *et al.* [27,30]. The aspect ratios, ζ, for Figs. 7(a), 7(c) and 7(d) are, respectively, 5.66, 3.31, and 3.05. It demonstrates that ζ is larger than π for reflexive separation, but smaller than π for coalescence. This is consistent with what we've observed in our experiments that the reflexive separation only occasionally appeared in the absence of magnetic field but commonly occurred with magnetic field, since in the absence of magnetic field ζ is just around critical threshold π so only sometimes reflexive separation occurs.

For all cases in Fig. 7, the spreading diameters D_y, lateral length D_x normalized by droplet diameter D and lateral velocity U_x, vertical velocity U_y normalized by relative velocity U in variance with time t are, respectively, shown in Figs. 8(a) and 8(b). We can observe that the maximum dimensionless spreading diameters $\widetilde{D_y}$ with and without magnetic field show little discrepancy, but the maximum dimensionless lateral lengths $\widetilde{D_x}$ show a big difference. In the compression phase, the inertia force dominates and the magnetic field doesn't have enough time to take obvious impact on $\widetilde{D_y}$. After that, the collision complex starts to reflex into a cylindrical structure with two bulbous ends, during which the motion inside the collision complex is almost along the x axis, which is perpendicular to magnetic field and would be influenced. Similarly, the dimensionless vertical velocities $\widetilde{U_y}$ with and without magnetic field show little discrepancy, but the dimensionless horizontal velocity $\widetilde{U_x}$ show a big difference for two cases. For no magnetic field case, when the spreading diameter D_y equals lateral length D_x, the dimensionless lateral velocity $\widetilde{U_x}$ is smaller than 1. However, under the influence of magnetic field, $\widetilde{U_x}$ spends less time reaching the peak value and goes higher (>1), and then declines in a smaller rate. It indicates the motion of lateral extension has indeed been promoted by magnetic field.

By choosing three different magnetic intensities, $\widetilde{D_y}$ and $\widetilde{D_x}$ in variance with t when We ≈ 50 are calibrated in Fig. 9. We can observe that $\widetilde{D_y}$ shows little difference for various magnetic intensities, but $\widetilde{D_x}$ shows an apparent discrepancy in the reflexive phase. This phenomenon is similar to the experimental results of a GaInSn droplet impacting on a glass plate by Yang *et al.* [24], which shows no great differences on initial spreading stages with and without magnetic field, but from the beginning of receding phase maximal spreading lengths along with and perpendicular to the direction of magnetic field show great difference, lending to an elliptical characteristic of spreading. It demonstrates that enough time is needed for magnetic field to have an effect.

In the compression phase, the maximal dimensionless spreading diameter ξ_y for different magnetic intensities varying from 0.1 T to 1.5 T when We ≈ 50 is plotted in Fig. 10(a), which shows ξ_y
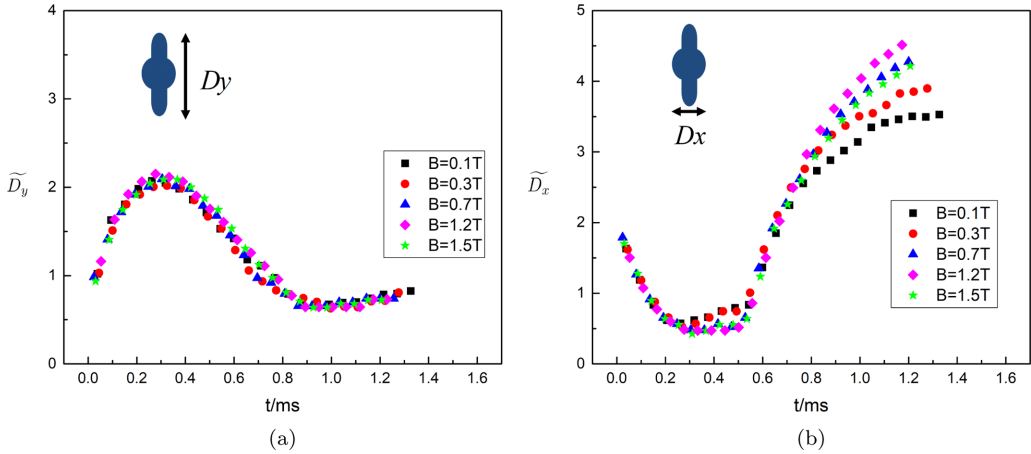
FIG. 9. The spreading diameters D_y and lateral length D_x normalized by droplet diameter D varies with time t for We ≈ 50.

is almost distributed around 2.1 to 2.3 and keeps nearly unchanged. Moreover, we've also provided an analysis of ξ_y in variance with the We number for 0.5 T, 1.0 T, and 1.5 T cases in Fig. 10(b). With the increase of We number, results under three magnetic intensities scatter closely around the correlation line and keep nearly the same trend with results in absence of magnetic field from Refs. [22,31]. Therefore, it also indicates that magnetic field has very little influence on ξ_y when N is very small($N < 0.4$).

In the reflexive phase, the maximum reflexive stretching length $D_{x(\max)}$ normalized by droplet diameter D, ξ_x, shows an increasing trend first and then a slow declining trend with increasing N, see Fig. 11(a). According to mass conservation law, it could be inferred that when magnetic intensity is enhanced, the average width of a collision complex along the z axis (the direction of magnetic field) decreases while the length along the x axis increases and length along the y axis keeps almost unchanged, which is consistent with Yang *et al.*'s [24] results that spreading perpendicular
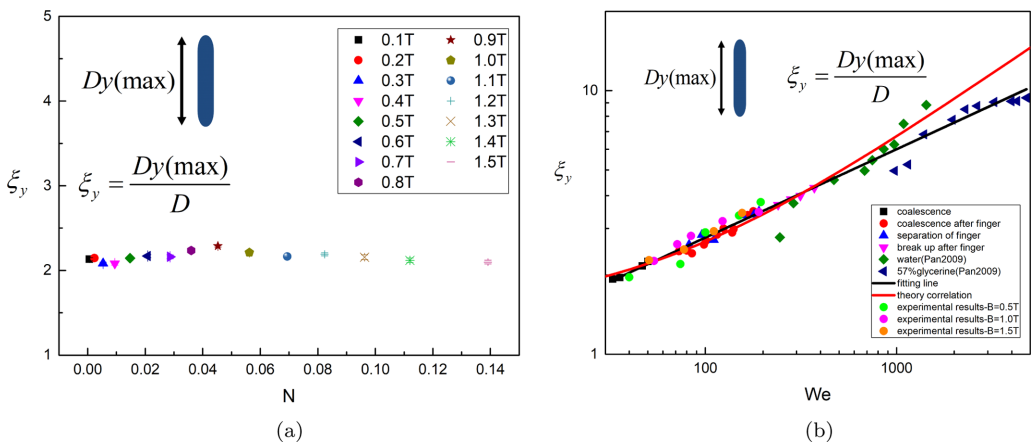

FIG. 10. (a) The dimensionless maximum spreading diameter ξ_y varies with magnetic parameter number N for We ≈ 50. (b) ξ_y varies with We for B $= 0.5$ T, 1.0 T, and 1.5 T, and the theoretical and fitting maximum dimensionless spreading diameter ξ_y in variance with We number are, respectively, We $= 24\xi_y^2 + 64\frac{1}{\xi_y} - 96$ and $\xi_y = 0.6$We$^{1/3}$, see details in Ref. [22].
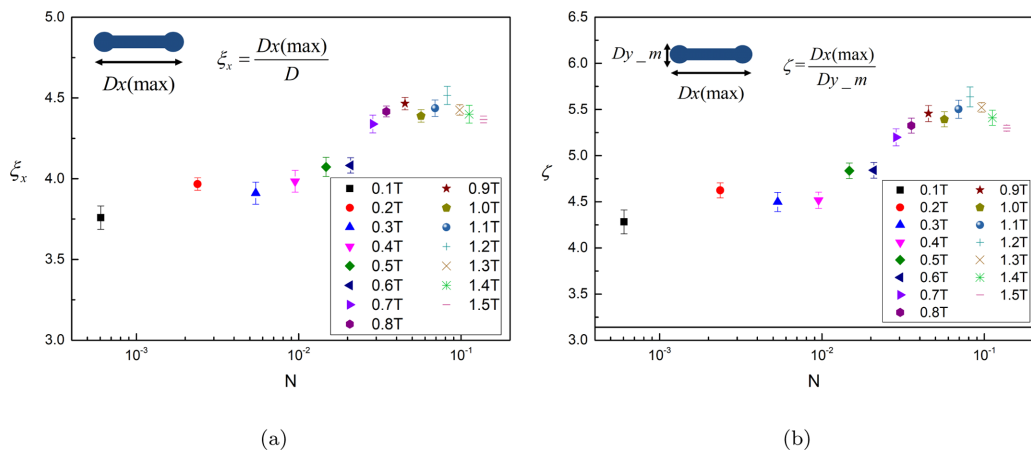
(a)

(b)

FIG. 11. (a) The maximum reflexive stretching length $D_{x(\max)}$ normalized by droplet diameter D, ξ_x, varies with magnetic interaction parameter N for We ≈ 50. (b) The maximum reflexive stretching length $D_{x(\max)}$ normalized by the vertical length at this moment D_{y_m}, ζ, varies with N for We ≈ 50.

to magnetic field is enhanced but reduced parallelly [24]. Furthermore, Qian and Law [32] have proposed that a nonuniform pressure field is set up within the lateral stretching structure, with inertial pressure of two ends higher than ligament. The pressure differential then generates a local flow which causes the ends to become bulbous and pull them toward the midsection. And during stretching, the flow inside the ligament moves toward bulbous ends. Under horizontal magnetic field, the flow in the bulbous end acts as a stretching force F_{Lorentz} and in ligament acts as a contracting force F_{Lorentz}', for bulbous ends to separate and the ligament to contract, as shown in the inset of Fig. 7(b). With magnetic intensity increasing, stretching electromagnetic forces would increase for collision complex to separate. Wang $et~al.$ [33] have numerically simulated the impact of a liquid metal droplet onto a thin film under both vertical and horizontal magnetic field. It demonstrates that the induced electric current inside shows a nonaxisymmetrical pattern when horizontal magnetic field is imposed, in contradiction with the perfectly circular current distribution for the vertical magnetic field case. Similarly, it could be inferred that the internal current and force distribution of binary droplet collision is also nonaxisymmetrical. However, in experiments, the three-dimensional, constantly changing velocity, induced electric current and Lorentz force distribution inside collision complex couldn't be gained, and limited space inhibits multispatial observation on the deformation process of droplet collision. It could be inferred that with increasing magnetic field the spreading contour of colliding droplets in the compression phase gradually tends to show an anisotropic pattern like an ellipse, and the receding process might take advantage of suppression along the minor axis of the ellipse and promote reflexive motion. When magnetic field is imposed, the electromagnetic force serves as a disturbance that leads to fragmentation of the cylindrical structure. The critical aspect ratio ζ shows a similar trend and keeps larger than π, see Fig. 11(b). It indicates that the lateral stretch always keeps in an unstable state and helps separate.

D. Influences of magnetic field on collision regimes

Given that collision regimes except reflexive separation show little difference from no magnetic field cases, to clearly figure out the influence of electromagnetic force, inertia, and surface tension, Fig. 12(a) shows the magnetic interaction parameter numbers N vary with We/48 for near head-on collisions of 0.5 T, 1.0 T, and 1.5 T. The parameter We/48 represents the ratio of initial kinetic energy and surface energy for two same-sized droplets, which was put forward by Jiang $et~al.$ [26] and widely used by Willis and Orme [34] and Planchette $et~al.$ [27]. It is observed that N gradually
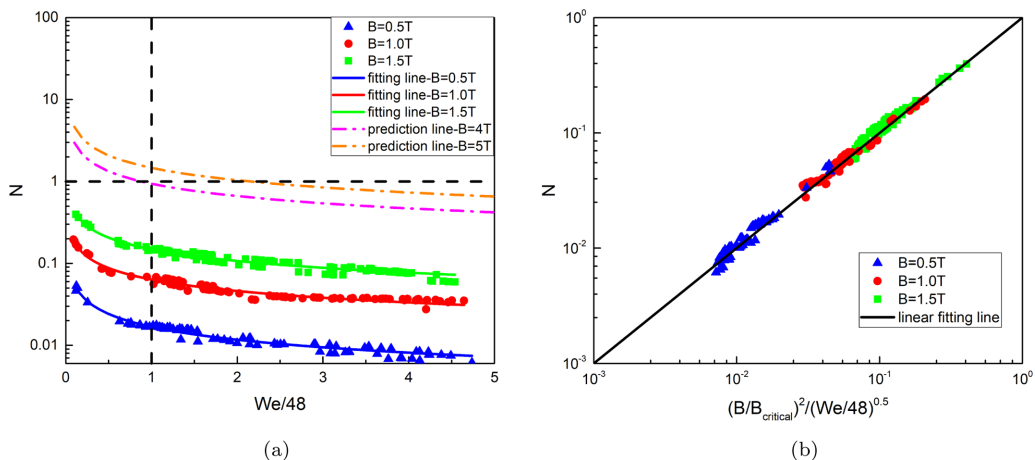
FIG. 12. (a) Magnetic parameter number N in variance with We/48 for near head-on collisions. (b) Magnetic parameter number N in variance with $(B/B_{critical})^2/(\mathrm{We}/48)^{0.5}$ for near head-on collisions, in which $B_{critical} = 4$ T.

decreases with the increasing We/48, which indicates that the effect of magnetic field weakens when the We number increases, and is far less than 1 for the these cases, which demonstrates that the ratio of electromagnetic force to inertia force is very small. The $N - \mathrm{We}/48$ map could be divided into four regions (shown in Table III): surface-tension dominated, inertia dominated, electromagnetic-force and surface-tension dominated, and electromagnetic-force and inertia dominated by the lines of $N{=}1$ and $\mathrm{We}/48 = 1$. Our experimental results are all located in surface-tension dominated and inertia-dominated regions, so magnetic field shows little influence on most of the collision regimes.

In detail, coalescence shown in the low We range (We/48 < 1) is surface-tension dominated, where inertia is only of secondary importance so electromagnetic force is even negligible. And the three collisional regimes, (coalescence after finger, separation of finger, and breakup after finger), in relatively high We range (We/48 > 1) are inertia dominated, for which the influence of magnetic field is increasingly smaller. Even though inertial forces of the three regimes increase compared to coalescence, the electromagnetic forces are still too small to make a difference. In addition, the acting time is another key factor of MHD effects. Zhang *et al.* [23] proposed that when magnetic field is imposed, the electromagnetic force acts on a timescale of

$$\tau = \rho/(\sigma_e B^2). \qquad (3)$$

By inletting $B {=}1.5$ T, we can get $\tau \approx 0.86$ ms, which is closest to the 15th snapshot with red rectangle in Fig. 4. We can observe that collision outcomes of all the other collision regimes except reflexive separation have almost been determined at this moment. For regimes except coalescence, there isn't enough acting time of magnetic field due to increased We numbers. For near head-on regimes with large We numbers, after the compression phase and finger generation the collision process would quickly be accomplished by contraction and oscillation; and for large

TABLE III. Region division of $N - \mathrm{We}/48$ map.

Region	N	We/48	Dominated
Upper left	>1	<1	Electromagnetic force and surface tension
Down left	<1	<1	Surface tension
Upper right	>1	>1	Electromagnetic force and inertia
Down right	<1	>1	Inertia

impact parameter X, the occurrence of stretching separation could also be determined quickly after impact, leading to inadequate acting time for magnetic field. Therefore, in the parameter range of our experiments, the effects of magnetic field nearly seem insignificant on the collision regimes in low (We/48 < 1) and high (We/48 > 1) range. However, for reflexive separation, there is enough acting time due to its particular deformation process of compression and reflexive phases, which makes it last a longer time than others. Large deformation interacts with the magnetic lines, and hence the motion of the collision complex will receive more variation in magnetic flux than other regimes, and more significant MHD effect is suffered consequently.

The fitting lines for 0.5 T, 1.0 T, and 1.5 T cases plotted in Fig. 12(a) could be, respectively, shown in the following forms:

$$N = 0.01681(\text{We}/48)^{-0.52425}, \quad B = 0.5 \text{ T}, \tag{4}$$

$$N = 0.06348(\text{We}/48)^{-0.46493}, \quad B = 1.0 \text{ T}, \tag{5}$$

$$N = 0.14843(\text{We}/48)^{-0.47299}, \quad B = 1.5 \text{ T}. \tag{6}$$

We can observe that the three power exponents are all approximately equal to -0.5, but the coefficients are different, which should be determined by magnetic intensity. To further investigate this, N in variance with We/48 and B could be derived in the following form shown in Fig. 12(b):

$$N \approx \frac{(B/B_{\text{critical}})^2}{(\text{We}/48)^{0.5}}, \quad B_{\text{critical}} = 4 \text{ T}. \tag{7}$$

Based on Eq. (7), we've further plotted $N - \text{We}/48$ prediction lines for 4 T and 5 T, respectively, in Fig. 12(a). We could deduce that when B rises up to 4 T, N is equal to 1 for We/48 = 1, which is a critical point since inertia of collision here is not only equal to surface tension but also equal to electromagnetic force. From 4 T on, the correlation lines for higher magnetic field start rising up to electromagnetic-force and surface-tension dominated and electromagnetic-force and inertia-dominated regions. The magnetic field would possibly start to have obvious effects on collision regimes no matter in low We range or in high. Therefore, $B = 4$ T is a critical value for collision regimes to be obviously influenced by magnetic field.

When the intensity of magnetic field is larger than 4 T, we can imagine that for near head-on collisions, the collision process still includes two phases in general: compression phase and reflexive phase, as shown in Fig. 13. In the compression phase, part of the spreading velocity is perpendicular to the direction of magnetic field, while the other part of the spreading velocity is parallel to it. In the reflexive phase, the reflexive velocity is always perpendicular to the direction of magnetic field. Detailed collision processes are depicted in the following:

(a) For coalescence with low We number, no matter in small or large X range, it would still remain since electromagnetic force and surface tension dominate and both of them induce droplets merging into an entity. For coalescence in relatively large We number range and with small X, near head-on collision, it shows an anisotropic pattern with enhanced spreading along the perpendicular direction of magnetic field and inhibited spreading along the parallel direction in the compression phase. When there is still enough kinetic energy remaining in the reflexive phase for the complex reflexing into a cylinder with two rounded ends, coalescence and reflexive separation are both possible to take place. As long as the length-to-diameter ratio ζ of a liquid column is smaller than π, reflexive separation doesn't appear but coalescence occurs, with the colliding complex contracting into an entity.

(b) For reflexive separation, we infer that the spreading process in the compression phase should be suppressed along the magnetic field direction while enhanced along the perpendicular direction. The maximum outer spreading contour shows an anisotropic shape like an ellipse. In the reflexive phase, the flow inside the colliding complex is perpendicular to magnetic field so it is beneficial for the magnetic field to have an obvious influence on the deforming process. The outward F_{Lorentz} in the bulbous end and inward F_{Lorentz}' in ligament, details shown in the sixth inset of Fig. 7(b),
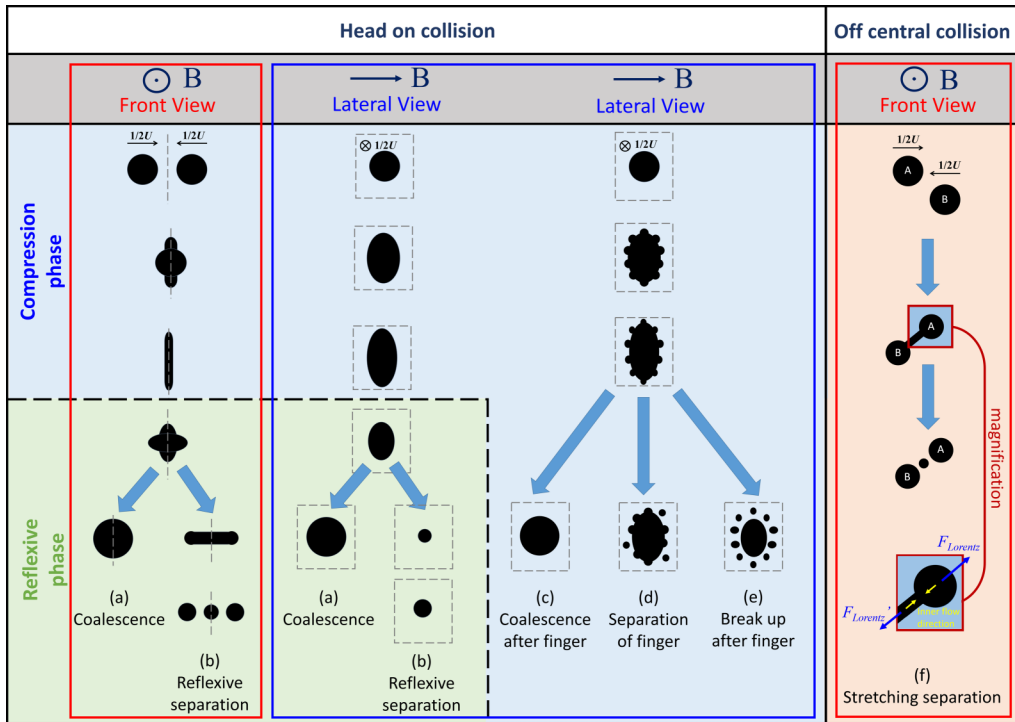
FIG. 13. Possible collisional process for large intensity of horizontal magnetic field ($B > 4$ T) (the grey dotted squares in lateral view are the cross-sectional drawing of grey dotted lines in front view).

promote the occurrence of reflexive separation. With increasing magnetic intensity, the onset We number of reflexive separation would show at smaller value. And the satellite droplet in the middle might become larger than the two bulbous droplets on both sides, and the one satellite droplet might separate into several smaller ones.

(c) For coalescence after finger, the spreading characteristics in the compression phase are similar to the aforementioned regimes. The maximum spreading contour shows an ellipse shape with thicker fingers along the parallel direction of magnetic field and thinner fingers in the perpendicular direction. The number of fingers in the parallel direction of magnetic field is less than the number in the perpendicular direction.

(d) For collisions of separation of finger, the second reflexive separation rarely exists. The influence of magnetic field focuses on the compression phase and the maximum spreading contour shows an ellipse shape with thinner but more fingers in the perpendicular direction of magnetic field and thicker but less fingers in the parallel direction. Due to the retraction motion along the direction of magnetic field, the separation of fingers appears earlier in the perpendicular direction than in parallel.

(e) For collisions of breakup after finger, the collision process is similar to that of separation of finger. More satellite droplets with smaller size might appear and separate in the perpendicular direction of magnetic field earlier in comparison with less satellite droplets with larger size in parallel direction.

(f) For stretching separation of large X, magnetic field might induce a stretching force F_{Lorentz} in the bulbous end and an inner contraction force $F_{\text{Lorentz}'}$ in the ligament. With increasing magnetic intensity, the inner satellite generated from the ligament in the middle of two bulbous ends might be larger than cases without magnetic field. The transition lines between stretching separation and other collision outcomes would move downward compared with cases without magnetic field.

IV. CONCLUSION

Binary collision dynamics of GaInSn droplets under the influence of horizontal magnetic field has systematically been characterized by varying the magnetic intensity within 1.5 T, with We number ranging from 5 to 200. Six different types of collision outcomes have been identified and the characteristics of these regimes are well shown by a series of time-resolved images. Results could be summarized in the following aspects:

(1) Magnetic field has obvious influences on reflexive separation of liquid metal droplets for small intensity ($B < 1.5$ T). Even though reflexive separation is only occasionally observed in the absence of magnetic field, it occurs commonly in the presence of magnetic field. Different from other collisions, reflexive separation includes two phases: compression and reflexive phases. The collision process lasts a longer time and the motion of collision complex in the reflexive phase is always perpendicular to magnetic field in this paper.

(2) For reflexive separation, the dimensionless lateral length $\widetilde{D}_x$ under different magnetic intensities shows some discrepancy in the reflexive phase, which might result from the outward Lorentz force induced by inward flow inside the collision complex. For small magnetic interaction parameter ($N < 0.4$), the dimensionless maximum lateral length ξ_x of reflexive separation shows an increasing trend first and then a slow declining trend with N, and the length-to-diameter ratio ζ remains larger than π in an unstable state easy to separate, while the dimensionless maximum spreading diameter ξ_y shows little discrepancy from the cases without magnetic field. Based on the contrast GaInSn droplets' results of reflexive separation without magnetic field, the empirical onset We number correlation presented by Gotaas *et al.* [25] for different liquids is amended via adding liquid metal results of GaInSn and mercury with smaller Oh numbers.

(3) Magnetic field does not play a significant role in the other collisional regimes except reflexive separation for $N < 0.4$. For near head-on collisions, N-We/48 map is presented to interpret why there is little influence of magnetic field on collision regimes. Moreover, it also predicts possible remarkable influences might appear if the magnetic intensity B could be raised greater than a critical value of 4 T, where N is equal to 1 at We/48 $= 1$. Magnetic intensity B is also related to the acting timescale τ of electromagnetic force: with increasing intensity, electromagnetic acting timescale τ decreases, leading to enough acting time of electromagnetic force before collision process accomplishes. To sum up, two requirements for magnetic field to have an obvious influence on droplet collision are enough acting time of magnetic field and great deformation perpendicular to the direction of magnetic field.

(4) When the intensity of magnetic field is larger than 4 T, near head-on collisions might show an anisotropic pattern in the compression phase, with enhanced spreading along the perpendicular direction of magnetic field and inhibited spreading along the parallel direction. In the reflexive phase, magnetic field would promote the separation of complex and induce earlier onset appearance of reflexive separation. When We number increases, collision regimes of coalescence after finger, separation of finger, and breakup after finger might show an ellipse shape with thinner but more fingers in the perpendicular direction of magnetic field and thicker but less fingers in the parallel direction. More satellite droplets with smaller size might appear and separate earlier in the perpendicular direction of magnetic field in comparison with less satellite droplets with larger size in the parallel direction. Meanwhile, the transition lines between stretching separation and other collision outcomes would move downward compared with cases without magnetic field.

[1] M. A. Abdou, A. Ying, N. Morley, K. Gulec, S. Smolentsev, M. Kotschenreuther, S. Malang, S. Zinkle, T. Rognlien, P. Fogarty *et al.*, On the exploration of innovative concepts for fusion chamber technology, Fusion Eng. Des. **54**, 181 (2001).

[2] G. G. van Eden, V. Kvon, M. C. M. Van De Sanden, and T. W. Morgan, Oscillatory vapour shielding of liquid metal walls in nuclear fusion devices, Nat. Commun. **8**, 192 (2017).

[3] J. P. Allain and C. N. Taylor, Lithium-based surfaces controlling fusion plasma behavior at the plasma-material interface, Phys. Plasmas **19**, 056126 (2012).

[4] A. Sterl, Numerical simulation of liquid-metal MHD flows in rectangular ducts, J. Fluid Mech. **216**, 161 (1990).

[5] N. B. Morley, S. Smolentsev, L. Barleon, I. R. Kirillov, and M. Takahashi, Liquid magneto-hydrodynamics–recent progress and future directions for fusion, Fusion Eng. Des. **51**, 701 (2000).

[6] I. Konkashbaev and A. Hassanein, Mhd problems in free liquid surfaces as plasma-facing materials in magnetically confined reactors, Fusion Eng. Des. **61**, 223 (2002).

[7] S. Smolentsev, R. Moreau, L. Bühler, and C. Mistrangelo, MHD thermofluid issues of liquid-metal blankets: phenomena and advances, Fusion Eng. Des. **85**, 1196 (2010).

[8] A. Vertkov, I. Lyublinski, M. Zharkov, G. Mazzitelli, M. L. Apicella, and M. Iafrati, Liquid tin limiter for FTU tokamak, Fusion Eng. Des. **117**, 130 (2017).

[9] G. Miloshevsky and A. Hassanein, Modeling of macroscopic melt layer splashing during plasma instabilities, J. Nucl. Mater. **415**, S74 (2011).

[10] P. Fiflis, M. Christenson, M. Szott, K. Kalathiparambil, and D. N. Ruzic, Free surface stability of liquid metal plasma facing components, Nucl. Fusion **56**, 106020 (2016).

[11] H. Bolt, V. Barabash, W. Krauss, J. Linke, R. Neu, S. Suzuki, N. Yoshida, and ASDEX Upgrade Team, Materials for the plasma-facing components of fusion reactors, J. Nucl. Mater. **329**, 66 (2004).

[12] B. Bazylev, I. Landman, A. Loarte, N. S. Klimov, V. L. Podkovyrov, and V. M. Safronov, Experiments and modeling of droplet emission from tungsten under transient heat loads, Phys. Scr. **2009**, 014061 (2009).

[13] B. Lipschultz, J. W. Coenen, H. S. Barnard, N. T. Howard, M. L. Reinke, D. G. Whyte, and G. M. Wright, Divertor tungsten tile melting and its effect on core plasma performance, Nucl. Fusion **52**, 123002 (2012).

[14] A. Hassanein and I. Konkashbaev, Macroscopic erosion of plasma facing and nearby components during plasma instabilities: The droplet shielding phenomenon, J. Nucl. Mater. **290**, 1074 (2001).

[15] D. G. Whyte, T. E. Evans, C. P. C. Wong, W. P. West, R. Bastasz, J. P. Allain, and J. N. Brooks, Experimental observations of lithium as a plasma-facing surface in the DIII-D tokamak divertor, Fusion Eng. Des. **72**, 133 (2004).

[16] J. Rudolph and G. Miloshevsky, Analysis and modeling of lithium flows in porous materials, Plasma Phys. Rep. **44**, 685 (2018).

[17] M. A. Jaworski, S. P. Gerhardt, N. B. Morley, T. Abrams, R. Kaita, J. Kallman, H. Kugel, R. Majeski, and D. N. Ruzic, Macroscopic motion of liquid metal plasma facing components in a diverted plasma, J. Nucl. Mater. **415**, S985 (2011).

[18] Z. H. Wang, X. Jia, and M. J. Ni, Effect of the magnetic field and current orientation on the splashing of liquid metal free surface of fusion reactor pfcs, Nucl. Fusion **58**, 126011 (2018).

[19] A. Menchaca-Rocha, F. Huidobro, A. Martinez-Davalos, K. Michaelian, A. Perez, V. Rodriguez, and N. Carjan, Coalescence and fragmentation of colliding mercury drops, J. Fluid Mech. **346**, 291 (1997).

[20] S. Y. Xia and C. B. Hu, Numerical investigation of head-on binary collision of alumina droplets, J. Propul. Power **31**, 416 (2015).

[21] C. Hu, S. Xia, C. Li, and G. Wu, Three-dimensional numerical investigation and modeling of binary alumina droplet collisions, Int. J. Heat Mass Transf. **113**, 569 (2017).

[22] X. Jia, J. C. Yang, J. Zhang, and M. J. Ni, An experimental investigation on the collision outcomes of binary liquid metal droplets, Int. J. Multiphase Flow **116**, 80 (2019).

[23] J. Zhang, T. Y. Han, J. C. Yang, and M. J. Ni, On the spreading of impacting drops under the influence of a vertical magnetic field, J. Fluid Mech. **809**, R3 (2016).

[24] J. C. Yang, T. Y. Qi, T. Y. Han, J. Zhang, and M. J. Ni, Elliptical spreading characteristics of a liquid metal droplet impact on a glass surface under a horizontal magnetic field, Phys. Fluids **30**, 012101 (2018).

[25] C. Gotaas, P. Havelka, H. A. Jakobsen, H. F. Svendsen, M. Hase, N. Roth, and B. Weigand, Effect of viscosity on droplet-droplet collision outcome: Experimental study and numerical comparison, Phys. Fluids **19**, 102106 (2007).

[26] Y. J. Jiang, A. Umemura, and C. K. Law, An experimental investigation on the collision behaviour of hydrocarbon droplets, J. Fluid Mech. **234**, 171 (1992).

[27] C. Planchette, H. Hinterbichler, M. Liu, D. Bothe, and G. Brenn, Colliding drops as coalescing and fragmenting liquid springs, J. Fluid Mech. **814**, 277 (2017).

[28] L. Rayleigh, On the capillary phenomena of jets, Proc. R. Soc. London **29**, 71 (1879).

[29] N. Ashgriz and J. Y. Poo, Coalescence and separation in binary collisions of liquid drops, J. Fluid Mech. **221**, 183 (1990).

[30] C. Planchette, E. Lorenceau, and G. Brenn, The onset of fragmentation in binary liquid drop collisions, J. Fluid Mech. **702**, 5 (2012).

[31] K. L. Pan, P. C. Chou, and Y. J. Tseng, Binary droplet collision at high weber number, Phys. Rev. E **80**, 036301 (2009).

[32] J. Qian and C. K. Law, Regimes of coalescence and separation in droplet collision, J. Fluid Mech. **331**, 59 (1997).

[33] J. J. Wang, J. Zhang, M. J. Ni, and R. Moreau, Numerical study of single droplet impact onto liquid metal film under a uniform magnetic field, Phys. Fluids **26**, 122107 (2014).

[34] K. Willis and M. Orme, Binary droplet collisions in a vacuum environment: an experimental investigation of the role of viscosity, Exp. Fluids **34**, 28 (2003).